Electrical and magnetic properties of $Nb_2O_{5-\delta}$ crystallographic shear structures

R. J. Cava, B. Batlogg, J. J. Krajewski, H. F. Poulsen, P. Gammel, W. F. Peck, Jr., and L. W. Rupp, Jr.
AT&T Bell Laboratories, Murray Hill, New Jersey 07974
(Received 28 May 1991)

The reduced niobium oxides $Nb_{25}O_{62}$, $Nb_{47}O_{116}$, $Nb_{22}O_{54}$, and $Nb_{12}O_{29}$ have been prepared in pure polycrystalline form by a niobium-metal gettering technique. They are related to the high niobia parent structure through the action of cystallographic shear to accommodate oxygen deficiency in $Nb_2O_{5-\delta}$. Electrical conductivities increase with increasing reduction: $Nb_{12}O_{29}$ is a metallic conductor down to 0.3 K. All show, surprisingly, Curie-Weiss behavior in the χ-vs-T curves, with $Nb_{12}O_{29}$ ordering antiferromagnetically at 12 K.

INTRODUCTION

At the heart of the controversy about the microscopic origin of superconductivity in copper oxides is whether or not the antiferromagnetism associated with the single-hole Cu^{2+} $3d^9$ state is of fundamental importance. To test whether unconventional spin-mediated superconductivity might be electron/hole symmetric, oxides of the elements with single electrons in the d state, such as Ti^{3+} $3d^1$, Nb^{4+} $4d^1$, and W^{5+} $5d^1$ are of particular interest. Localized magnetic spin states and magnetic ordering have, in fact, never been reported in transition-metal oxides with single filling of the $4d$ or $5d$ states, because of the preference for conventional d-band conductivity or for metal-metal bonding. On exploring the possibility of a d^1-d^9 and ferroelectricity-superconductivity relationship in oxides (see, for instance, Ref. 1), we have been studying the properties of slightly reduced niobium oxides. These "crystallographic shear" structures are derived from insulating $4d^0Nb_2O_5$ by removal of rows of oxygen atoms, introducing small amounts of $4d^1$ niobium $4+$. Small amounts of Nb-based crystallographic shear structures have been previously synthesized for structural or thermodynamic studies, but they have apparently never been synthesized in sufficient purity to study the physical properties of single-phase materials. We have been able to synthesize many of them by a metal gettering technique. We have found that both antiferromagnetic spin correlations and conductivity are introduced at very low Nb^{4+} contents, ultimately resulting in metallic conductivity and antiferromagnetic ordering at 12 K for the most reduced member of the series, $Nb_{12}O_{29}$, where the doping level is 0.17 Nb^{4+}. This is the first time, to our knowledge, that magnetic ordering has been observed in a niobium-based oxide.

The superconducting copper oxide perovskites are remarkable in their well-known ability to accommodate relatively large amounts of oxygen deficiency without the breakdown of their crystal structures. This is by no means the rule for metal oxides based on the corner sharing of coordination polyhedra, and is possible only due to the variety of coordination geometries which copper can tolerate when bonded to oxygen. For the highly charged early transition-metal oxides, in which sixfold (or higher) metal-oxygen coordination is preferred, point oxygen defects are energetically unfavorable and a different mechanism is required to accommodate variability in oxygen stoichiometry. For these metal oxides with three-dimensional blocks of corner-shared MO_6 octahedra as the basic structural component, it is not possible to remove significant amounts of oxygen without causing a structural rearrangement in which the blocks are broken along a plane of shared corners. The block parts are then shifted to eliminate whole rows of oxygen atoms, forming a shear plane of now edge-shared octahedra. Such shear planes cannot form in a random fashion; rather, they form long-range-ordered arrays along the edges of ReO_3-type blocks. Continuous variation of oxygen content is not possible. Rather, a series of compounds of distinct, well-defined metal to oxygen stoichiometries is found, with multiple-phase mixtures of the individual compounds at intermediate overall oxygen contents (see, for instance, Refs. 2 and 3).

The electrical properties of TiO_x, VO_x, MoO_x, and WO_x reduced phases have been well studied, no doubt in part because of the relative ease of materials preparation.[4] The reduced niobium oxides were studied extensively by crystallographers during the development of the understanding of crystallographic shear structures. For niobium oxides, many distinct long-range-ordered structures are known[5,6] at compositions Nb_2O_5 ($NbO_{2.50}$), $Nb_{53}O_{132}$ ($NbO_{2.49}$), $Nb_{25}O_{62}$ ($NbO_{2.48}$), $Nb_{47}O_{116}$ ($NbO_{2.47}$), $Nb_{22}O_{54}$ ($NbO_{2.45}$), and $Nb_{12}O_{29}$ ($NbO_{2.42}$). The physical properties of individual members of this family of crystallographic shear structures, derived from reduction of Nb_2O_5, have never before been characterized, although resistivity and optical measurements on NbO_x samples which had not been structurally characterized have been previously reported.[7]

All of the $NbO_{2.5-\delta}$ structures can be derived by the joining of blocks of corner-shared NbO_6 octahedra of size $n \times m \times \infty$ along planes of shared edges, with, in some instances, NbO_4 tetrahedra inserted to help fill space. The high-temperature form of insulating Nb_2O_5, for instance, is made by $3\times4\times\infty$ and $3\times5\times\infty$ blocks of NbO_6 octahedra, with some tetrahedra as shown in Fig. 1.

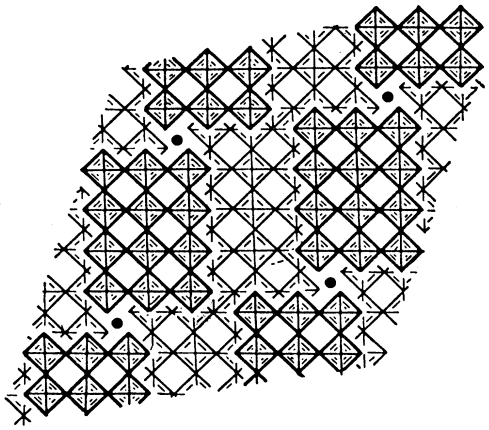

FIG. 1. The idealized crystal structure of Nb_2O_5, NbO_6 octahedra are shown, as well as tetrahedrally coordinated Nb by closed or open circles. Bold octahedra are on a level $\frac{1}{2}$ octahedron height above the background octahedra. The structure repeats infinitely perpendicular to the plane of the figure, to form long columns of corner-shared octahedra dressed by planes of edge-shared octahedra. The planes of edge-shared octahedra occur at the location in the structure where the bold and background octahedra meet, and extend perpendicular to the plane of the paper.

$Nb_{12}O_{29}$, the last of the series, has $3\times4\times\infty$ blocks of octahedra, without tetrahedra, as shown in Fig. 2. In the real crystal structures, the niobium-oxygen octahedra are irregular in bond length and bond angle, characteristic of ferroelectriclike structural distortions.[8–10] The more complex compounds, for example, with formulas $Nb_{53}O_{132}$ and $Nb_{47}O_{116}$, consist of long-range alternation, on the unit cell level, of the simpler block structures. $Nb_{47}O_{116}$ for instance (Fig. 3), consists of a 1:1 perfectly ordered alternation of $Nb_{22}O_{54}$ and $Nb_{25}O_{62}$. It is be-

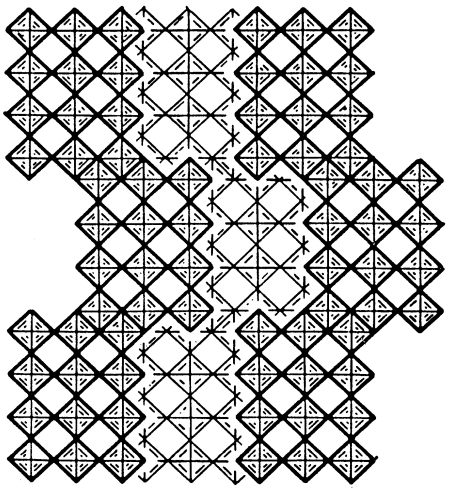

FIG. 2. The idealized crystal structure of orthorhombic symmetry $Nb_{12}O_{29}$. Detailed description as in Fig. 1.

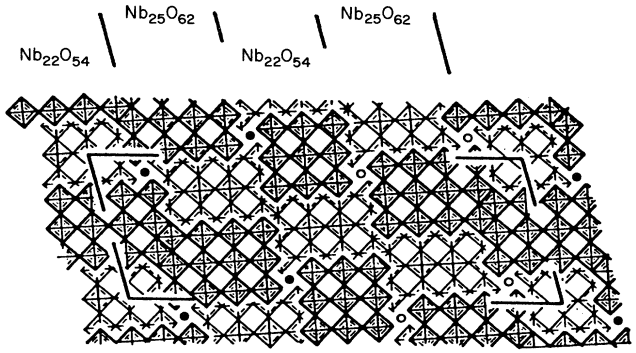

FIG. 3. The idealized crystal structure of $Nb_{47}O_{116}$. It is an ordered, unit cell scale intergrowth of the two simpler compounds $Nb_{25}O_{62}$ and $Nb_{22}O_{54}$. Detailed description as in Fig. 1.

cause of the crystallographic complexity of the NbO_x crystallographic shear structures and the renewed interest in the electrical properties of oxides that we decided to investigate their synthesis and electrical properties. Here we present a new straightforward technique for preparing $Nb_2O_{5-\delta}$, to synthesize the crystallographic shear structure compounds $Nb_{25}O_{62}$, $Nb_{47}O_{116}$, $Nb_{22}O_{54}$ and $Nb_{12}O_{25}$ in single-phase form, and report the characterization of their electrical and magnetic properties.

SYNTHESIS

We have synthesized $Nb_2O_{5-\delta}$ by a gettering technique similar to that found to be successful in $YBa_2Cu_3O_{7-\delta}$.[11] First, ceramic pellets of spec-pure Nb_2O_5 (99.999%) were fired in air at 1375 °C for several hours. This densifies the pellets, but only to approximately 80% of theoretical density. Half pellets (approximately 0.5 g) were then sealed in evacuated quartz tubes with Nb-metal powder (200 mesh), separated from direct contact with the metal by $\frac{1}{2}$-in. quartz spacers. Samples were then heated at 1300, 1200, or 900 °C for three days and quickly cooled to room temperature at the end of the annealing process by removing from the furnace while hot. Preliminary experiments indicated that Nb to Nb_2O_5 weight ratios between 0.0 and 0.08 were sufficient to span the range of phases existing between Nb_2O_5 and NbO_2 at these temperatures. Because the phases are very close in [Nb]:[O] ratio, very fine intervals and careful Nb to Nb_2O_5 weight measurements were necessary to synthesize the crystallographic shear structures in pure form.

The surface of the samples were first sanded (SiC) to remove any remnant of Nb powder accidentally adhering. Oxygen content of the gettered samples was determined by measuring the gain in weight of the reduced samples on heating in air for 2 h at 800 °C to restore the samples to Nb_2O_5 ($NbO_{2.5}$):

$$NbO_x+(2.5-x)O=NbO_{2.5}\ .$$

The variation of final oxygen content with initial Nb to Nb_2O_5 weight ratio is shown in Fig. 4. The eventual sat-

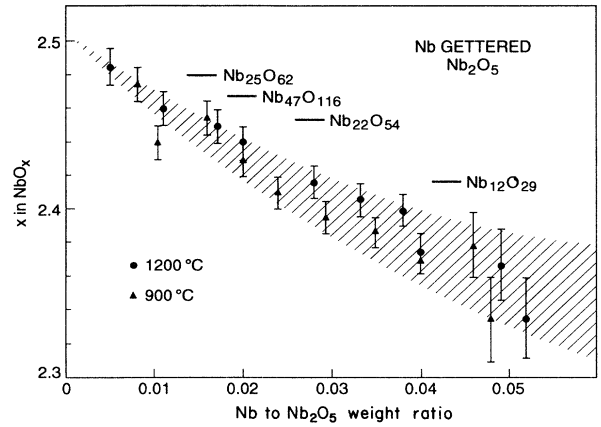

FIG. 4. Variation of final [O]:[Nb] ratio in samples of initial composition Nb_2O_5 ([O]:[Nb] = 2.5) annealed at 900 and 1200 °C as a function of initial Nb-metal powder getterer to Nb_2O_5 weight ratio.

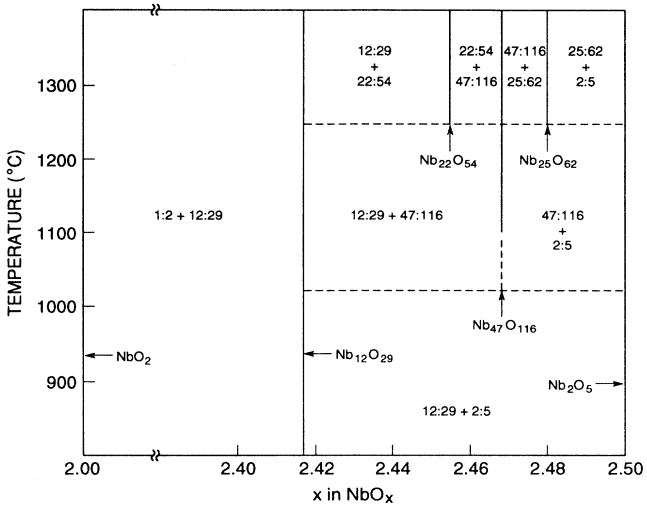

FIG. 5. Approximate phase diagram for NbO_x based on our gettering experiments at 900, 1200, and 1300 °C.

uration of the oxygen content of the samples with increasing Nb to Nb_2O_5 weight ratio indicates a decreasing efficiency of the Nb-metal gettering for higher oxygen-deficiencies. Although the trend in final oxygen content with gettering ratio is clear, scatter in the results occurs in different synthesis runs because at such fine scales of metal-oxygen ratio (much finer than one worries about in $Ba_2YCu_3O_{7-\delta}$) small differences in the sample and Nb powder geometry influence the details of the final outcome.

The stoichiometries $Nb_{25}O_{62}$, $Nb_{47}O_{116}$, $Nb_{22}O_{54}$, and $Nb_{12}O_{29}$ are marked on Fig. 4. To determine which phases were formed in the gettered annealing, powder x-ray diffraction patterns were recorded between 4 and 50° 2Θ with Cu $K\alpha$ radiation. The diffraction patterns for the materials prepared at 900 °C indicate that the only phases present for [Nb]:[O] ratios between 1:2.5 and 1:2.3 are Nb_2O_5, $Nb_{12}O_{29}$, and NbO_2, at [Nb]:[O] ratios of 1:2.5, 1:2.42, and 1:2. At intermediate oxygen stoichiometries, the samples are two phase mixtures of either Nb_2O_5 and $Nb_{12}O_{29}$, or $Nb_{12}O_{29}$ and NbO_2. For the materials prepared at 1200 °C, the phases present are Nb_2O_5, $Nb_{47}O_{116}$, $Nb_{12}O_{29}$, and NbO_2, again with distinct two-phase mixtures at intermediate compositions. We find it surprising that $Nb_{47}O_{116}$ can be formed at a lower temperature than either $Nb_{25}O_{62}$ or $Nb_{22}O_{54}$, from which it is derived. At 1300 °C, the phases present are Nb_2O_5, $Nb_{25}O_{62}$, $Nb_{47}O_{116}$, $Nb_{22}O_{54}$, and NbO_2. We see no evidence under these conditions for the formation of the shear structures $Nb_{53}O_{132}$ or Nb_3O_7 (which would be the Nb^{4+} and Nb^{5+} analog of $TiNb_2O_7$). A summary of these data in phase-diagram form is presented in Fig. 5. The results at 1300 °C are in good agreement with those obtained by reduced oxygen pressure synthesis,[5] except that $Nb_{53}O_{132}$ could apparently be made single phase under limited synthetic conditions.

TABLE I. Unit cells for $Nb_2O_{5-\delta}$ crystallographic shear structures.

Composition	O/Nb	a	b	c	β	Symmetry	Block size(s)	Source
H.T. Nb_2O_5	2.500	21.08	3.823	19.33	119.8°	$P2$	$3\times4\times\infty$, $3\times5\times\infty$	a,b
$Nb_{25}O_{62}$	2.480	29.78	3.825	21.14	94.7°	$C2$	$3\times4\times\infty$	a,c
$Nb_{47}O_{116}$	2.468	57.74	3.823	21.18	105.3°	$C2$	$3\times3\times\infty$, $3\times4\times\infty$	a,d
$Nb_{22}O_{54}$	2.455	17.86	3.82	31.50	102.1°	$P2$	$3\times3\times\infty$, $3\times4\times\infty$	e
$Nb_{12}O_{29}$	2.417	28.90	3.83	20.72	—	Amma	$3\times4\times\infty$	f

[a]A. D. Wadsley and S. Andersson, in *Perspectives in Structural Chemistry,* edited by J. D. Dunitz and A. Ibers (Wiley, New York, 1970), p. 1.
[b]Powder diffraction file, Card 16-53.
[c]Powder diffraction file, Card 22-40 for $AlNb_{49}O_{124}$.
[d]Powder diffraction file, Card 23-447.
[e]R. Norin, M. Carlsson, and B. Elgquist, Acta Chem. Scand. **20**, 2892 (1966).
[f]R. Norin, Acta Chem. Scand. **17**, 1391 (1963).

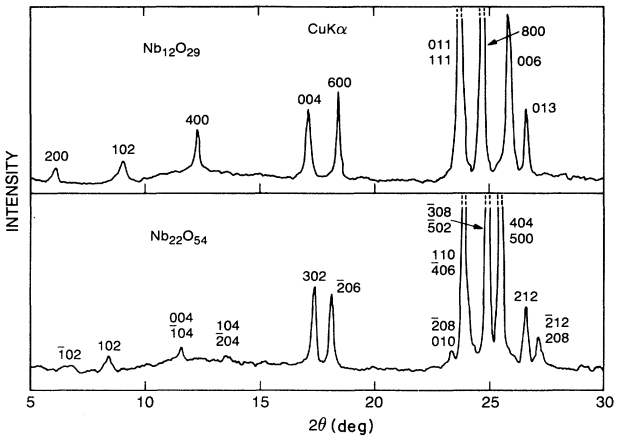

FIG. 6. Characteristic portions of the powder x-ray diffraction patterns for $Nb_{22}O_{54}$ and $Nb_{12}O_{29}$, Cu $K\alpha$ radiation.

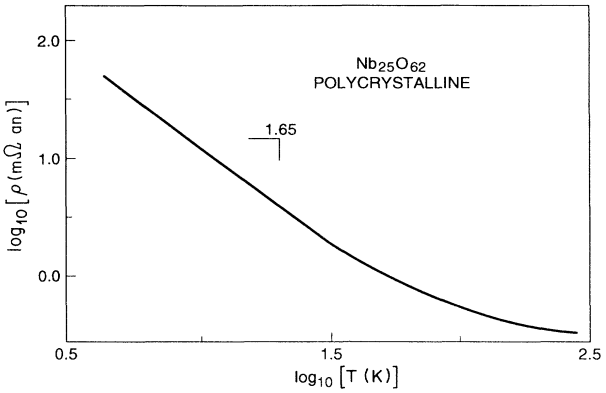

FIG. 7. The temperature-dependent resistivity of $Nb_{25}O_{62}$.

Because the crystallographic unit cells of the $Nb_2O_{5-\delta}$ crystallographic shear structures are large and of low symmetry, and the crystal structures are so strongly related, their powder x-ray diffraction patterns are complex and quite similar. Conclusive identification of the phases through powder x-ray diffraction therefore required careful analysis. A summary of the structural data employed for phase identification is presented in Table I. For all phases excluding $Nb_{22}O_{54}$, indexed powder diffraction patterns can be found in the literature. The best diffraction peaks for phase identification are below 30° 2Θ when Cu $K\alpha$ radiation is employed. Figure 6 compares as examples the powder x-ray diffraction patterns for orthorhombic $Nb_{12}O_{29}$ and monoclinic $Nb_{22}O_{54}$. We have indexed the latter based on the published cell dimensions. Table I also includes a column of entries for the different ReO_3-type corner-shared block sizes found in the synthesized compounds. For $Nb_{12}O_{29}$, the material is purely of the orthorhombic symmetry form when prepared at 1300 °C; in the lower-temperature preparations, a small amount of the monoclinic symmetry form of $Nb_{12}O_{29}$ is also present.

RESISTIVITY

The temperature-dependent resistivities of single-phase polycrystalline pellets of the crystallographic shear compounds were measured below 300 K in four-probe bar geometry. Nb_2O_5, in which all Nb is in its highest oxidation state, is a white, insulating material. The room-temperature resistivity measured on a polycrystalline pellet prepared in air at 1325 °C was 3×10^4 Ω cm. Reduction of the average Nb valence through removal of oxygen and formation of the various shear structures decreases the resistivities until $Nb_{12}O_{29}$ is reached (average Nb valence = 4.83), which has a metallic ρ of T down to 0.3 K. The colors change from light blue grey to blue black. On further reduction, NbO_2 is formed, which is a poor conductor. The resistivities measured at 300 and 50 K are presented in Table II. The measurements on polycrystalline pellets include some contribution from the grain boundaries, so one would expect the resistivities of single crystals to be lower. Note the decrease in resistivity of (at least) five orders of magnitude on decreasing the average Nb valence from 5.00 to 4.96 on going from Nb_2O_5 to $Nb_{25}O_{62}$.

Plots of the temperature-dependent resistivities are presented in Figs. 7–11. For $Nb_{25}O_{62}$, resistivity in-

TABLE II. Electrical and magnetic properties of niobium oxide crystallographic shear structures.

	ρ (Ω cm)[a]		$\chi=\chi_0+C/(T+\Theta_{CW})$[b]		
Compound	300 K	50 K	χ_0 (emu)	Θ (K)	C (emu K)
Nb_2O_5	3×10^4	—	—	—	—
$Nb_{25}O_{62}$	3×10^{-1}	1.5	0.9×10^{-5}	0	0.7×10^{-2}
$Nb_{47}O_{116}$	1.6×10^{-2}	3.6×10^{-2}	1.3×10^{-5}	7	1.1×10^{-2}
$Nb_{22}O_{54}$	1.5×10^{-2}	1.6×10^{-2}	-0.1×10^{-5}	12	2.2×10^{-2}
$Nb_{12}O_{29}$	4×10^{-3}	2×10^{-3}	1×10^{-5}	24	2.7×10^{-2}
$Ti_{0.5}Nb_{11.5}O_{29}$	1.2×10^{-2}	1.0×10^{-2}	1.1×10^{-5}	18	1.9×10^{-2}

[a]Resistivities measured on polycrystalline pellets.
[b] All values per mole NbO_x or $(Nb,Ti)O_x$.

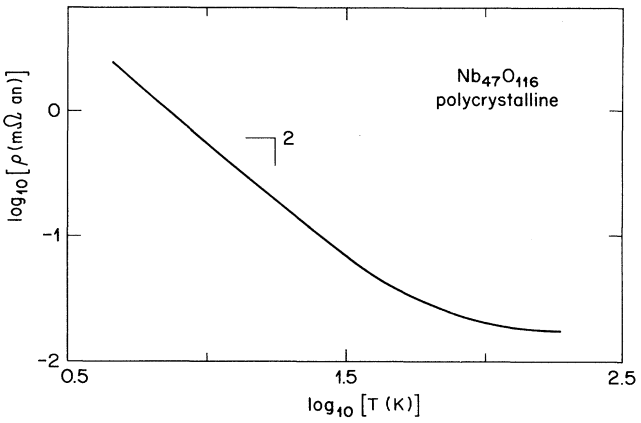

FIG. 8. The temperature-dependent resistivity of $Nb_{47}O_{116}$.

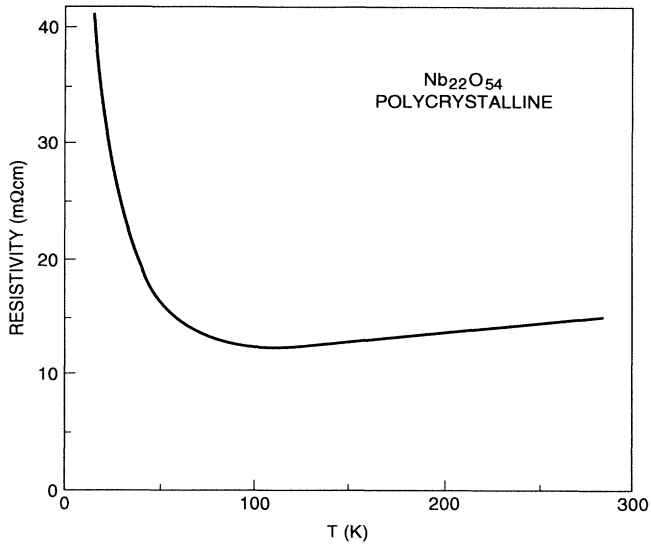

FIG. 10. The temperature-dependent resistivity of $Nb_{22}O_{54}$.

creases continuously with decreasing temperature from 300 K. Plotting the data as $\log\rho$-vs-$1/T$, $\log\rho$-vs-T, or $\log\rho$-vs-$T^{1/4}$ did not yield straight-line behavior in any temperature range for either $Nb_{25}O_{62}$ or $Nb_{47}O_{116}$. We have therefore represented the data on $\log\rho$-vs-$\log T$ plots, which show linear regions for both materials below 30 K (Figs. 7 and 8). The power-law behavior, with powers of 1.6 and 2.0 for $Nb_{25}O_{62}$ and $Nb_{47}O_{116}$, respectively, might be due to three-dimensional localization. For $Nb_{47}O_{116}$ (average Nb valence 4.94) a small temperature region of metallic conductivity is observed down to approximately 240 K, shown on linear scales in Fig. 9. For the next most reduced material, $Nb_{22}O_{54}$ (average Nb valence 4.91), the 300-K resistivity is similar to that of $Nb_{47}O_{116}$, but the metallic region extends down to approximately 100 K, where the resistivity again begins to increase with decreasing temperature (Fig. 10).

Finally, for $Nb_{12}O_{29}$, the last in the series, the resistivity shows a metallic temperature dependence from 300 down to 0.3 K (Fig. 11). At approximately 25 K the resistivity begins to decrease more rapidly than it does at higher temperatures. At 12 K there is a kink where the resistivity drops more sharply, then flattens out at very low temperatures. The decrease in resistivity occurs where the material undergoes a transition to an antiferromagnetic state at 12 K. Thus spin- induced scattering of the conduction electrons made a significant contribution to the resistivity above the ordering temperature. In the $3d^1$ antiferromagnetic compounds Sr_2VO_4 (Refs. 12 and 13) and $CeTiO_3$ (Ref. 14), for comparison, the resistivity is unaffected (semiconducting Sr_2VO_4) or there is a metal-semiconductor transition ($CeTiO_3$) at the magnetic ordering temperature.

We have attempted to substitute Ti and W in small amounts in the Nb-based crystallographic shear structures, particularly in $Nb_{12}O_{29}$. For W substitutions up to 25% in $(Nb,W)O_x$, many reduced, crystallographic shear

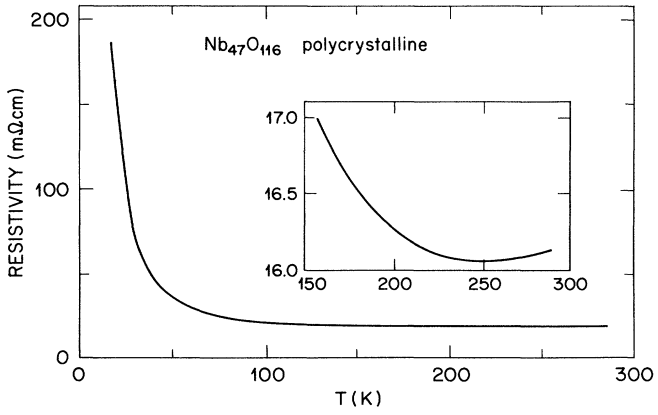

FIG. 9. The temperature-dependent resistivity of $Nb_{47}O_{116}$, linear scales. Inset: resistivity detail near 300 K.

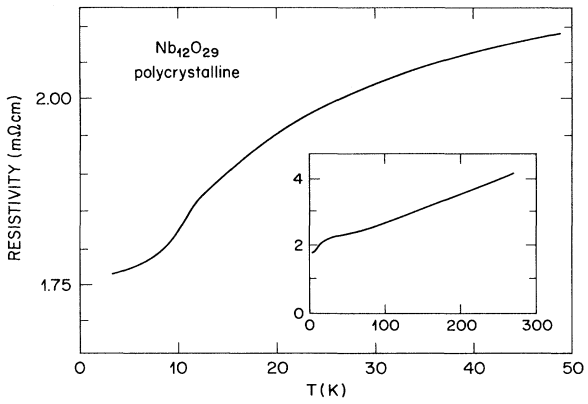

FIG. 11. The temperature-dependent resistivity of $Nb_{12}O_{29}$ in the vicinity of the magnetic ordering temperature. Inset: resistivity between 300 and 4 K.

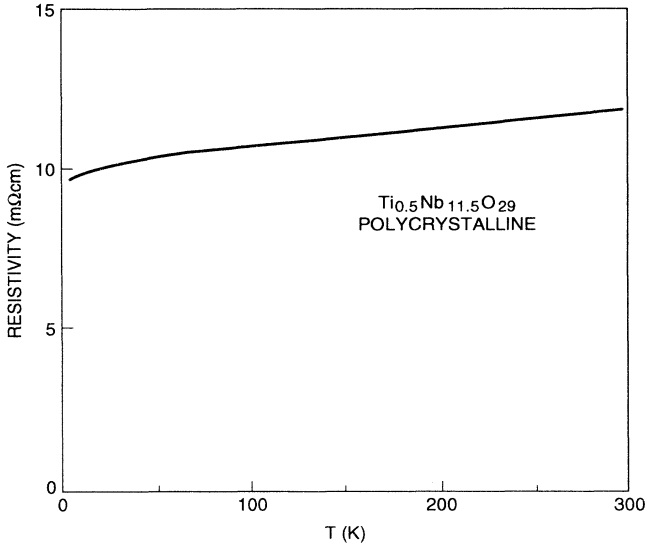

FIG. 12. The temperature-dependent resistivity of $Nb_{11.5}Ti_{0.5}O_{29}$.

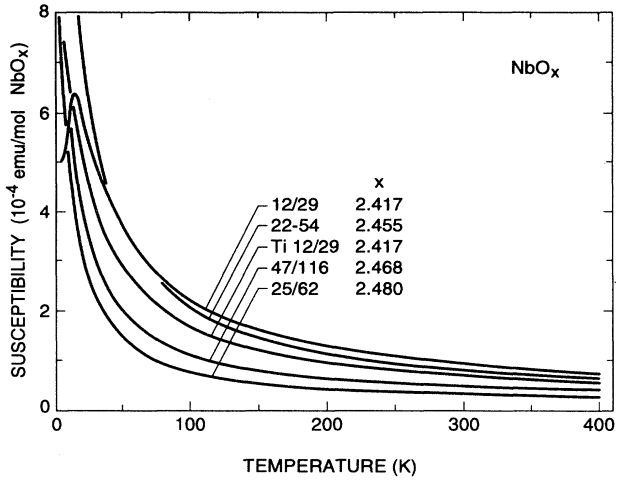

FIG. 13. Magnetic susceptibilities of $Nb_{25}O_{62}$, $Nb_{47}O_{116}$, $Nb_{22}O_{54}$, $Nb_{12}O_{29}$, and $Ti_{0.5}Nb_{11.5}O_{29}$ plotted per mole $(Nb,Ti)O_x$.

type phases are formed which contain both W and Nb, but none had metallic conductivity and they were not pursued further. We were not able to partially substitute W for Nb in $Nb_{12}O_{29}$ by the gettered synthetic technique we have described. The Ti^{4+} and Nb^{5+} analogs of $Nb_{25}O_{62}$ and $Nb_{12}O_{29}$, $TiNb_{24}O_{62}$ and $Ti_2Nb_{10}O_{29}$, are known compounds. We therefore studied partial Ti substitution in $Nb_{12}O_{29}$ to determine its effect on the electrical conductivity and magnetic ordering. The temperature-dependent resistivity of $Nb_{11.5}Ti_{0.5}O_{29}$ is presented in Fig. 12. The resistivity has increased over that of $Nb_{12}O_{29}$ by approximately a factor of 5 and the material is now only marginally metallic. In this material, half of the $4d^1$ Nb^{4+} has been replaced by magnetically and electrically inert $3d^0$ Ti^{4+}. There is no resistive signature of a magnetic transition. This material is not superconducting down to 1.4 K.

MAGNETIC PROPERTIES

Magnetic susceptibilities were measured in a field of 10 kOe in a commercial SQUID magnetometer. In Figs. 13 and 14 we present the magnetic susceptibilities of $Nb_{25}O_{62}$, $Nb_{47}O_{116}$, $Nb_{22}O_{54}$, $Nb_{12}O_{29}$, and $Ti_{0.5}Nb_{11.5}O_{29}$, plotted per mole NbO_x, in order to normalize to one Nb per formula unit. For magnetic systems with localized moments, the magnetic susceptibility above the ordering temperature is described in terms of the formula $\chi=\chi_0+C/(T+\Theta_{CW})$, where C is the Curie constant and Θ_{CW} is the Curie-Weiss temperature. Θ_{CW} is zero for noninteracting spins, positive for antiferromagnetic spin interactions, and negative for ferromagnetic spin interactions. All samples tested showed a small temperature-independent contribution to the susceptibility (χ_0) which we attribute to the near cancellation of core diamagnetism, Van Vleck contributions, and the paramagnetism of the free carriers. χ_0 has been subtracted from χ before plotting Fig. 14.

The data show that even very dilute mixture of Nb^{4+} into the crystallographic shear structures results in inducing a localized magnetic moment. (Nb_2O_5 displays a weak, temperature-independent diamagnetism.) The very good linearity of the $1/(\chi-\chi_0)$-vs-T data indicate that the moments are well localized. The Curie-Weiss fitting parameters are presented in Table II. The materials

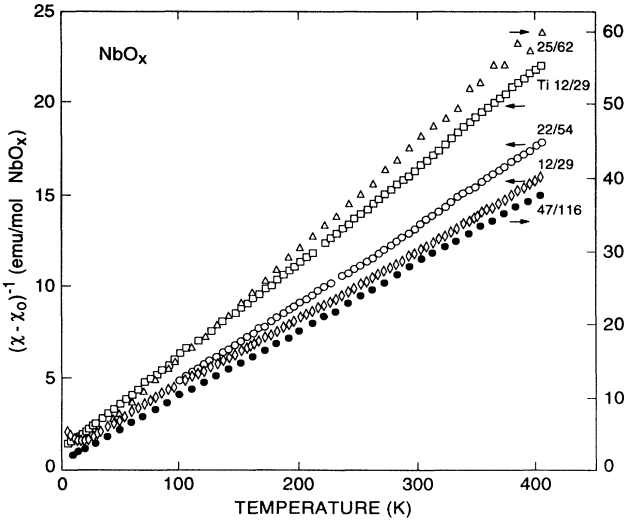

FIG. 14. Inverse magnetic susceptibility of $Nb_{25}O_{62}$, $Nb_{47}O_{116}$, $Nb_{22}O_{54}$, $Nb_{12}O_{29}$, $Ti_{0.5}Nb_{11.5}O_{29}$ plotted per mole $(Nb,Ti)O_x$. Small temperature-independent terms (χ_0) have been subtracted from the data before plotting.

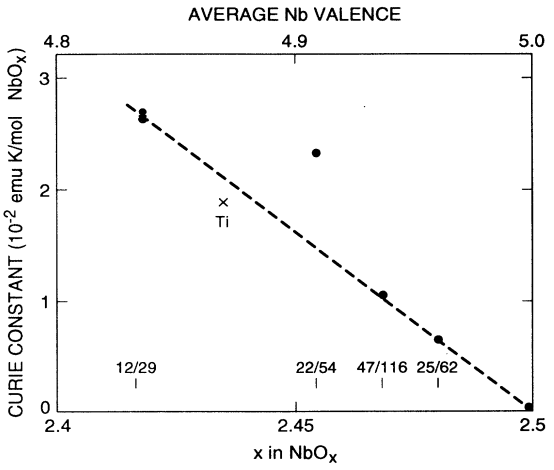

FIG. 15. Moment calculated from $1/(\chi-\chi_0)$ vs T for all NbO_x shearer structures synthesized in this study, as a function of oxygen content or average Nb valence.

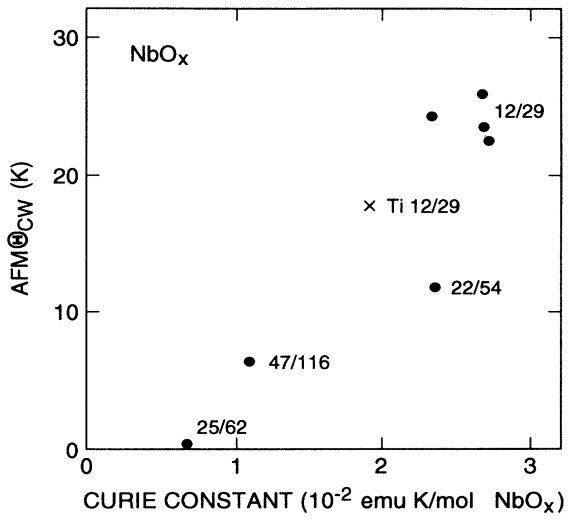

FIG. 16. Correlation of Θ_{CW}, the Curie-Weiss temperature, and C, the effective moment, for Nb_nO_m crystallographic shear structures.

display an increasing Curie constant (C), proportional to the number of moments and an increasing Curie-Weiss temperature (Θ_{CW}), indicative of increasing antiferromagnetic interactions, as the Nb^{4+} content increases.

Figure 15 shows the moment calculated from $1/\chi$ vs T for all the shear structures studied, as a function of oxygen content in NbO_x or formal average Nb valence. Within experimental error the plot is linear, indicating that as Nb^{4+} with its $4d^1$ configuration is introduced into the structures, its moment, although apparently not the full one, is constant. The slope of the curve is 0.8 μ_B/Nb^{4+}, or approximately half that which is expected. Of course these materials are electrical conductors, so some fraction of the one $4d$ electron per Nb^{4+} must be delocalized to give rise to conductivity and not local moment magnetism. Figure 16 shows that Θ_{CW} and C likewise appear to be linearly related: As the magnetic moment per Nb increases, the strength of the magnetic interactions also increases.

All materials were tested for magnetic ordering down to 2 K, but only $Nb_{12}O_{29}$ orders. The result for $Nb_{22}O_{54}$ is particularly interesting because its Curie-Weiss temperature is 12 K. In the simplest models, the antiferromagnetic ordering temperature is expected to be close to Θ_{CW}, but is usually found to be lower. The fact that $Nb_{22}O_{54}$ does not order above $\Theta_{CW}/6$ suggests that either frustration of spins or two-dimensional interactions are present. In Fig. 17 we present the inverse magnetic susceptibility of $Nb_{12}O_{29}$ between 5 and 400 K, plotted per mole $NbO_{2.417}$. For the sample in Fig. 17 $\chi_0=9.3\times10^{-6}$ emu/mol $NbO_{2.417}$, which has been subtracted from the data before plotting. The figure shows that the data follow perfectly the Curie-Weiss behavior expected for antiferromagnetic interactions with a Curie-Weiss temperature $\Theta_{CW}=24$ K. The variation of Θ_{CW} from sample to sample is approximately ±1.5 K. The antiferromagnetic ordering is seen in the departure of $1/\chi$ from the linearity at low temperatures. Fitting from 30–400 K yields $C=2.67\times10^{-2}$ emu K/mol and $\Theta_{CW}=24$ K.

The antiferromagnetic transition is shown in detail in Fig. 18, plotted as χ vs T. The extrapolation of the Curie-Weiss behavior at higher temperatures is shown by the dashed line. The data show that the antiferromagnetic transition occurs near 12 K, and also that deviation from the Curie-Weiss behavior occurs for temperature up to 25 K. The fact that the antiferromagnetic fluctuations are observed to begin near the Θ_{CW} temperature but that the actual ordering does not occur until approximately half of Θ_{CW} suggests again that either frustration of spins or two-dimensional interactions are involved in deter-

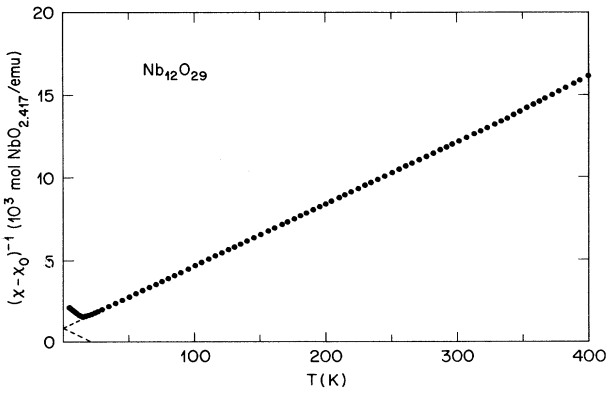

FIG. 17. The inverse magnetic susceptibility of $Nb_{12}O_{29}$ measured in a field of 10 kOe, plotted per mole $NbO_{2.417}$. A small constant term, $\chi_0=9.3\times10^{-6}$ emu/mol, has been subtracted. From the linear extrapolation, an interaction temperature Θ_{CW} of 24 K is deduced.

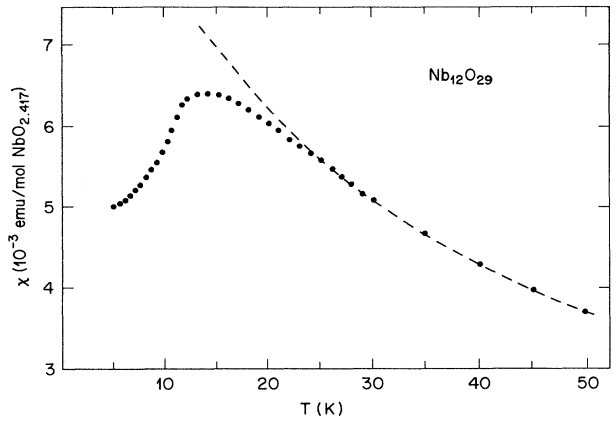

FIG. 18. Detail of the magnetic susceptibility of $Nb_{12}O_{29}$ in the region of the antiferromagnetic ordering temperature, plotted per mole $NbO_{2.417}$. The dashed line shows the extrapolation of the Curie-Weiss fit from high temperatures. Note the deviation from the Curie-Weiss behavior beginning near 25 K and the ordering transition near 12 K.

mination of the actual ordering temperature. Among the several samples of $Nb_{12}O_{29}$ studied, we find only a small variation of the low-temperature susceptibility. While the magnitude of the peak value varies from 5.2×10^{-3} to 6.3×10^{-3} emu/mol $NbO_{2.417}$, the steepest decrease of $\chi(T)$ is always between 11 and 12 K. In the samples

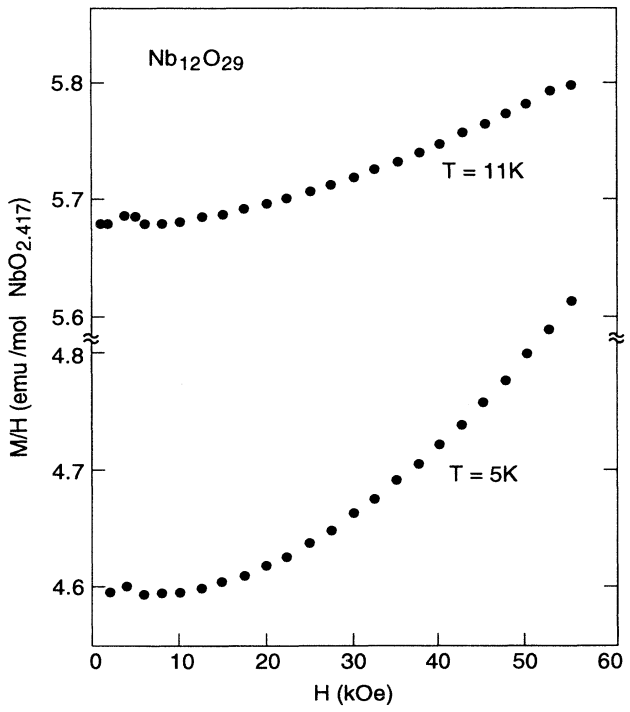

FIG. 19. Field dependence of M/H for $Nb_{12}O_{29}$ below the magnetic ordering temperature of 12 K.

prepared at 900 and 1300 °C, the transition is slightly more rounded than for samples prepared at 1200 °C.

Figure 19 presents the magnetic field dependence of M/H for $Nb_{12}O_{29}$ at 11 and 5 K. As expected for an antiferromagnet, high magnetic fields restrain the antiferromagnetic spin pairing and partially restore the moment from the Curie-Weiss behavior observed above the ordering temperature.

CONCLUSIONS

Detailed interpretation of the electrical and magnetic properties of these materials requires an understanding of their charge distribution. For $Nb_{12}O_{29}$, for example, the average Nb valence is 4.83. If the charges were localized, the material would be an insulator, and would be $Nb_2^{4+}Nb_{10}^{5+}O_{29}$. Niobium 4+ has an $S=1/2$, $4d^1$ configuration. $Nb_{12}O_{29}$ is a metallic conductor and remains metallic below the magnetic ordering temperature. The moment calculated from χ is only 42% of the value expected if all Nb^{4+} had the full magnetic moment, assuming for simplicity $s=1/2$ $g=2$. The results suggest that $Nb_{12}O_{29}$ could be an itinerant antiferromagnet. Itinerant antiferromagnets, however, would not commonly show as distinctive a Curie-Weiss behavior as we have observed for $Nb_{12}O_{29}$, which is a signature of localized spins, unless the bands are very narrow. The relative complexity of the crystal structure suggests an alternative interpretation. That is, that one particular set of Nb positions contains 4+ Nb with a localized $4d^1$ configuration, giving rise to the magnetism, and other sites contribute delocalized electrons, giving rise to the conductivity. $Nb_{12}O_{29}$ could therefore be analogous to the magnetic superconductors, such as $ErRh_4B_4$, where magnetism and superconductivity involve different subsets of electrons.

We have presented evidence to show that $Nb_{12}O_{29}$ is a metallic antiferromagnetic with an ordering temperature of 12 K. It is not superconducting down to 0.3 K. It is the first known niobium-oxide-based antiferromagnet. The mixed dimensionality of the crystal structure apparently appears in the magnetic properties through the reduction of the true ordering temperature to $\Theta_{CW}/2$. We have found that other members of the Nb_2O_5-derived reduced oxides, $Nb_{25}O_{62}$, $Nb_{47}O_{116}$, and $Nb_{22}O_{54}$, also display Curie-Weiss behavior in χ vs T, but do not magnetically order down to 2 K. Thus, antiferromagnetic interactions are a general property of reduced niobium oxide crystallographic shear structures. In particular, we do not find evidence for spin-paired polarons at low temperatures, as suggested in Ref. 7. Although some $3d$-shell-based reduced Ti and V oxides have been found to be antiferromagnetic,[11] the $4d$-based reduced Nb oxides have not previously shown any tendency toward local moment magnetism. The fact that such local moments can occur in reduced Nb-$4d$-based oxides suggests the existence of narrow electronic bands and poor metal-oxygen covalency. Further research is necessary to determine the degree of localization of the magnetic states, and to determine whether the magnetic transition in $Nb_{12}O_{29}$ is

of a spin-glass type. Niobium, being an early transition element, would not be expected to have the same degree of hybridization of its valence orbitals with oxygen as do the superconducting copper and bismuth oxides. Nevertheless, the Sr_xNbO_3 perovskites, which consist of solely corner-shared NbO_6 octahedra, are metallic conductors (not superconducting) presumably with the charge carriers in a band of primarily metal d character. The NbO_x crystallographic shear structures studied here consist primarily of perovskitelike blocks, but contain intersecting planes of octahedra which share edges with each other resulting in a relatively short Nb-Nb separation, suitable for direct metal orbital overlap. The charge carriers are therefore again likely to be in a Nb d orbital dominated band. We therefore can more generally propose that any niobium-oxygen-based superconductors are likely to be conventional metal d-band superconductors, such as is $LiTi_2O_4$, and would not have the kind of metal-oxygen covalency that makes copper- and bismuth-based oxides so special. More detailed study of the magnetic niobium oxides will be of interest in its own right, and may shed a more general light on the possible relationships between ferroelectricity, antiferromagnetism, and covalency in transition-metal oxides.

[1]K. A. Muller, Phase Trans. **22**, 5 (1990).
[2]R. S. Roth and A. D. Wadsley, Acta Crystallogr. **19**, 42–47 (1965).
[3]A. D. Wadsley and S. Andersson, in *Perspectives in Structural Chemistry,* edited by J. D. Dunitz and J. A. Ibers (Wiley, New York, 1970), Vol. 3, pp. 1–58.
[4]See, for instance, N. F. Mott, *Metal-Insulator Transitions* (Taylor and Francis, London, 1974).
[5]Shigeyuka Kimura, J. Solid State Chem. **6**, 438 (1973).
[6]J. F. Maruco, J. Chem. Phys. **70**, 649 (1979).
[7]C. Rüscher, E. Salje, and A. Hussain, J. Phys. C **21**, 3737 (1988).
[8]R. B. von Dreele and A. K. Cheetham, Proc. R. Soc. London, Ser. A **338**, 311 (1974).
[9]Rolf Norin, Acta Chem. Scand. **17**, 1391 (1963).
[10]A. D. Wadsley, Acta Crystallogr. **14**, 660 (1961).
[11]R. J. Cava, B. Batlogg, C. H. Chen, E. A. Rietman, S. M. Zahurak, and D. Werder, Phys. Rev. B **36**, 423 (1987).
[12]A. Nozak, H. Yoshikawa, T. Wada, H. Yamauchi, and S. Tanaka, Phys. Rev. B **43**, 181 (1991).
[13]M. J. Rey, P. Dehaudt, B. Lambert, J. L. Soubeyroux, J. Beille, M. Cyrot, G. Fillon, J. L. Tholence, and F. Cyrot-Lackmann, J. Solid State Chem. **85**, 321 (1990).
[14]D. A. MacLean and J. E. Greedan, Inorg. Chem. **20**, 1025 (1981).